Proceedings of the LHCP2015 Conference, St. Petersburg, Russia, August 31 - September 5, 2015

Editors: V.T. Kim and D.E. Sosnov

New Physics search in mono-jet final states with the ATLAS experiment at the LHC

GIULIANO GUSTAVINO

Universita e INFN, Roma-1, Piazzale Aldo Moro 5, 00185 Roma, Italy.

giuliano.gustavino@cern.ch

On behalf of the ATLAS Collaboration

Abstract. The search for New Physics in final states with an energetic jet and large missing transverse momentum plays a major role in the physics program of the LHC experiments. This experimental signature is sensitive to different New Physics models including different scenarios of supersymmetry, models that predict the existence of extra dimensions and the production of weakly interacting Dark Matter candidates. Results based on the LHC Run-1 dataset corresponding to 20.3 fb^{-1} and firsts performance plots based on the data collected at the center of mass energy of 13 TeV with the ATLAS experiment at the LHC are presented.

Motivations

The existence of Dark Matter (DM) particles [1] is a well-established hypothesis to explain a range of astrophysical and cosmological measurements. Since none of the known Standard Model (SM) particles provides suitable candidates for this kind of matter, several theories postulate the existence of new particles that are stable (or at least long-lived) and neutral, thus fulfilling two important requirements for being the DM in the universe. One class of particle candidates of interest for searches at the LHC consists of weakly interacting massive particles (WIMPs) [2]. These are expected to couple to Standard Model particles through a generic weak interaction, which could be the known weak interaction of the SM or a new type of interaction.

Since that WIMPs do not interact with the detector material, their production leads to signatures with missing transverse momentum ($p_{\mathrm{T}}^{\mathrm{miss}}$), the magnitude of which is called $E_{\mathrm{T}}^{\mathrm{miss}}$, and one can be tagged by the identification of a high energy jet in the final state. This event topology is particular interesting in a hadronic machine as LHC because can count on a higher expected rate and a higher sensitivity in most of the theoretical interpretations with respect to the other mono-X final states.

Mono-jet final states have been studied also in the context of searches for supersymmetric compressed scenarios, large extra spatial dimensions (LED) and invisible decays of the Higgs boson.

Run-1 Analysis

The final states in the mono-jet analysis [3] in the ATLAS experiment [4] consist of a limited number of jets with the leading one with very high p_{T} plus a large energy imbalance in the plane transverse to the colliding proton beams. The data are selected during the data taking using a trigger logic that selects events with high $E_{\mathrm{T}}^{\mathrm{miss}}$ as computed at the final stage of the three-level trigger system [5]. The event selection used in the analysis is summarized in Table 1.

The strategy adopted is based on the building of nine Signal Regions (SR), defined applying the lepton veto and lower $E_{\mathrm{T}}^{\mathrm{miss}}$ cut from 150 GeV to 700 GeV. Four Control Regions (CR) are defined kinematically close with the SR and requiring the presence of one or two isolated leptons in the final state. They are used in a simultaneous fit to evaluate the normalization factors associated to the dominant electroweak background V + jets (where $V = W/Z$) in the SR. The top and di-boson processes are estimated by MC simulations while the multi-jet background is based on the data.

TABLE 1. Event selection criteria applied for the selection of mono-jet like SRs. Taken from Ref. [3].

Selection criteria
Primary vertex
$E_{\mathrm{T}}^{\mathrm{miss}} > 150, ..., 700$ GeV
Jet quality requirements
At least one jet with $p_{\mathrm{T}} > 30$ GeV and $\|\eta\| < 4.5$
Lepton and isolated track vetoes
The leading jet with $p_{\mathrm{T}} > 120$ GeV and $\|\eta\| < 2.0$
Leading jet $p_{\mathrm{T}}/E_{\mathrm{T}}^{\mathrm{miss}} > 0.5$
$\Delta\phi(\mathrm{jet}, E_{\mathrm{T}}^{\mathrm{miss}}) > 1.0$

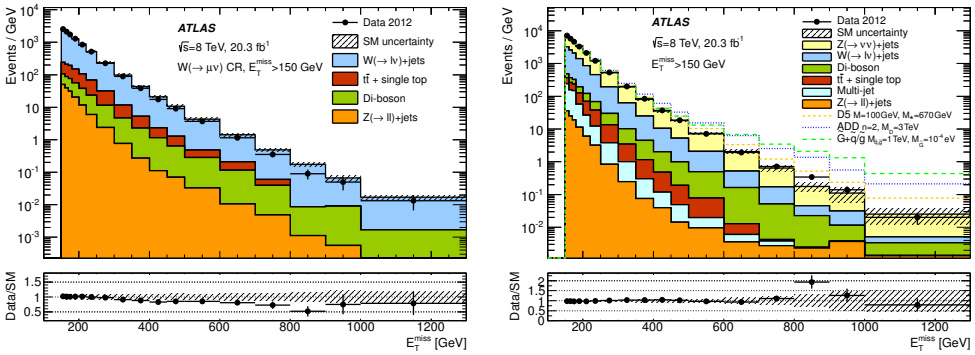

FIGURE 1. Data/MC comparison in the one muon CR (left) and in the SR with $E_{\mathrm{T}}^{\mathrm{miss}} > 150$ GeV (right) after the fit using the entire data sample of 20.3 fb^{-1} at $\sqrt{s} = 8$ TeV. The error bands in the ratios include the statistical and experimental uncertainties on the background expectations. Signal hypotheses in the DM, SUSY and LED scenarios are also plotted. Taken from Ref. [3].

In Figure 1 the SR and one muon CR are shown. This CR has a major role in the analysis because it is used to evaluate the main irreducible background $Z(\nu\nu)$ + jets through the $W(\mu\nu)$ + jets control sample, using the entire data sample at $\sqrt{s} = 8$ TeV corresponding to 20.3 fb^{-1}, thus allowing to reduce the systematical uncertainty on the $Z(\nu\nu)$ + jets background.

In general, a good agreement is observed between the data and the SM expectations (see Table 2). The largest difference between the number of events in data and the SM expectations is observed in the SR with $E_{\mathrm{T}}^{\mathrm{miss}} > 700$ GeV, corresponding to a 1.7σ deviation from the background-only hypothesis. The agreement between the data and the SM expectations for the total number of events in the different signal regions is translated into model-independent 95% confidence level (CL) upper limits on the visible cross section varying between 726 fb and 3.4 fb in several SRs.

TABLE 2. Data and SM background expectation in several SRs. For the SM expectations both the statistical and systematic uncertainties are included. Taken from Ref. [3].

SR (lower $E_{\mathrm{T}}^{\mathrm{miss}}$cut)	150 GeV	300 GeV	500 GeV	700 GeV
Observed events	364378	18020	1028	126
SM expectation	372100 ± 9900	18000 ± 500	1030 ± 60	97 ± 14
$Z \to \nu\nu$	217800 ± 3900	12800 ± 410	740 ± 60	71 ± 13
$W \to \tau\nu$	79300 ± 3300	2800 ± 200	130 ± 20	11 ± 3
$W \to e\nu$	23500 ± 1700	880 ± 80	43 ± 7	3 ± 1
$W \to \mu\nu$	28300 ± 1600	850 ± 80	35 ± 6	2 ± 1
$Z \to \mu\mu$	530 ± 220	7 ± 3	2 ± 1	1 ± 1
$Z \to \tau\tau$	780 ± 320	14 ± 6	0 ± 0	0 ± 0
$t\bar{t}$, single top	6900 ± 1400	200 ± 70	7 ± 7	0 ± 0
di-bosons	8000 ± 1700	690 ± 200	65 ± 35	8 ± 7
multi-jets	6500 ± 6500	44 ± 44	1 ± 1	0 ± 0

Interpretations

As just mentioned before, the mono-jet analysis is sensitive to a wide spectrum of theoretical interpretations so it is possible to intepret the model independent limits in the several scenarios to allow a comparison of the results with the other analyses and experiments.

Dark Matter scenarios

The interaction of WIMPs with Standard Model particles can be investigated in two different approaches: in the Effective Field Theory (EFT) and in the so called Simplified Models.

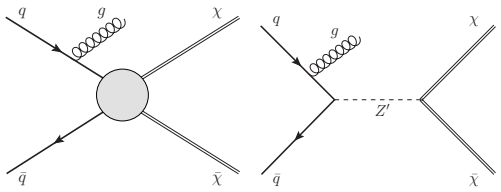

FIGURE 2. Feynman diagrams for the production of WIMP pairs $\chi\bar{\chi}$ associated with a jet from initial-state radiation of a gluon: a contact interaction described with effective operators (on the left) and a simplified model with a Z' boson (on the right). Taken from Ref. [3].

In the EFT context the processes are studied in a contact interaction scenario, and the DM production processes are mediated by a single new heavy particle with a mass M_{med} too large to be produced directly at the LHC and bigger than the DM mass m_χ ($M_{\text{med}} >> \sqrt{s} >> m_\chi$). In these hypotheses it is possible to integrate out the mediator in the process and probing the different scenarios choosing a particular operator that describes the kind of interaction (vectorial, axial, scalar, pseudo-scalar, tensorial etc.). Considering that no evidences and excesses are seen in the SRs it is possible to set the limits in several EFT scenarios. The limits on the signal strength are translated to bounds on the WIMP-nucleon scattering cross sections to compare the results with the direct search experiment ones.

Figure 3 demonstrates that the detection of DM candidates in a collider can give complementary results with respect to the direct (DAMA, LUX etc.) and indirect (AMS, Ice-Cube etc.) detection experiments and in particular in the low DM mass region where these detectors loose their sensitivity (currently the direct detection cannot reach the spectrum area below $\sim$ 3 GeV).

Besides the EFT operators, in the collider experiments the pair production of WIMPs is also investigated within the Simplified Models, where a pair of WIMPs couples to a pair of quarks explicitly via a new mediator particle (for example a Z'). The free parameters to constrain in this context are the mass and spin property of the mediator and of the DM particles, the width of the mediator and the vertex couplings $\sqrt{g_q\, g_\chi}$.

Figure 4 shows how, for a given mediator mass (in this specific case a Z' like mediator) and two values of the width Γ, the real value of the mass suppression scale would compare to the suppression scale $M_* = M_{\text{med}}/\sqrt{g_q\, g_\chi}$ value derived assuming a contact interaction (shown as dashed lines). In this case the contact interaction regime is reached for M_{med} values larger than 5 TeV. In the intermediate range the contact interaction approach would't be the proper choice. In fact, the bounds would be underestimated in the middle region (in 700 GeV $< M_{\text{med}} <$ 5 TeV) with respect to the actual values because the mediator would be produced resonantly and the actual M_* value is higher than in the contact interaction regime. Instead, in the small mediator mass regime below 700 GeV, the M_* limits would be optimistic and overestimated because the WIMP would be heavier than the mediator, and WIMP pair production via this mediator would thus be kinematically suppressed.

It is also possible to constrain the couplings $\sqrt{g_q\, g_\chi}$ of the simplified model vertex in the plane of mediator and WIMP mass (M_{med} versus m_χ) as shown in left plot in Figure 4. Within this model, the regions above the relic density (as measured by the WMAP satellite, assuming annihilation in the early universe in the absence of any interaction other than the one considered) line lead to values of the relic density larger than measured and are excluded.

Other interpretations

The mono-jet final states have been studied also in the other theoretical contexts getting stringent constrains to the models investigated.

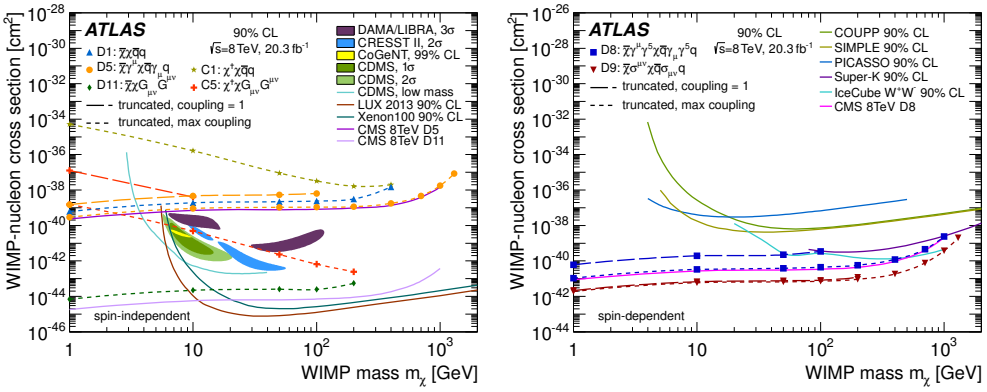

FIGURE 3. Inferred 90% CL limits on the spin-independent (left) and spin-dependent (right) WIMP-nucleon scattering cross section as a function of DM mass m_χ for different operators. Results from direct-detection experiments for the spin-independent cross section, and the CMS (untruncated) are shown for comparison. Taken from Ref. [3].

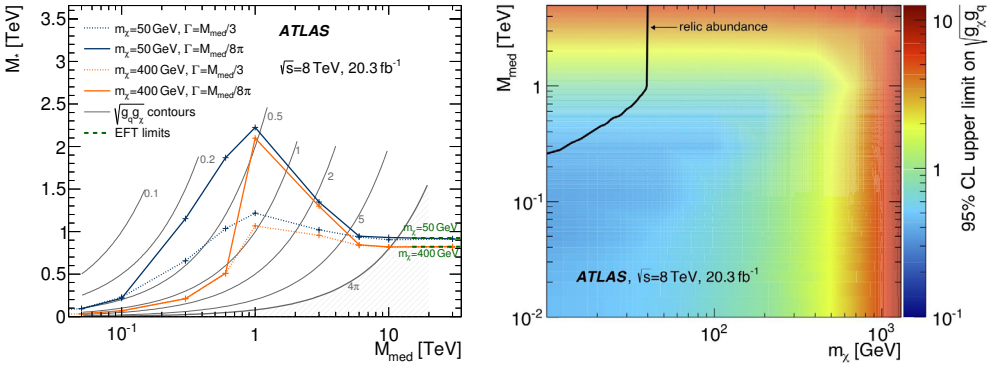

FIGURE 4. Left: comparison between the limits in the plane (M_{med}, M_*) in the EFT and simplified model approach choosing two m_χ and Γ hypotheses. Right: upper limit on the couplings $\sqrt{g_q\, g_\chi}$ in the plane (M_{med}, m_χ). In both the figure is it used a Z' like mediator model. More informations in the text. Taken from Ref. [3].

Several SUSY compressed scenarios can lead to a mono-jet like topology. The Run-1 results are expressed in limits on the cross-section for the dominant associated production of a Gravitino and a gluino (or a squark) , $pp \to \tilde{G}\tilde{g}(\tilde{q}) + X$, decaying into a quark (gluon) in association with a Gravitino, $\tilde{g}(\tilde{q}) \to \tilde{G}g(q)$ [6]. The limits on the Gravitino mass $m_{\tilde{G}}$ in the cases of degenerate and non-degenerate squarks and gluinos scenarios are also computed. In Figure 5 the cross-section times efficiency as a function of the squark/gluino mass for different $m_{\tilde{G}}$ in the degenerate squarks and gluinos scenario and different gravitino masses for the SR with $E_{\text{T}}^{\text{miss}} > 500$ GeV are shown and compared with the corresponding model-independent limits.

The large extra dimensions theory would aim to provide a solution to the mass hierarchy problem by postulating the presence of n extra spatial dimensions of size R, and defining a fundamental Planck scale in $4 + n$ dimensions, M_D, given by ${M_{\text{Pl}}}^2 \sim {M_D}^{2+n} R^n$ [7]. In this scenario the graviton modes may escape detection and its production in association with a jet taking to a mono-jet signature. In this context the scenarios with several number of extra dimensions are investigated. The predicted product of cross section, acceptance and efficiency, for the SR with $E_{\text{T}}^{\text{miss}} >$ 500 GeV as a function of M_D, for n = 2, n = 4, and n = 6 is shown in Figure 5 (the bands represent the theory uncertainty). For comparison, the model-independent observed (solid line) and expected (dashed line) 95% CL limits on the cross section are also plotted.

Finally, the mono-jet analysis can give competitive and important results in the invisible Higgs decays interpretation since that the study of the Higgs boson properties does not exclude a sizeable branching ratio [8]. The Higgs scalar field could also play an important role in describing the interaction between dark and ordinary matter in the

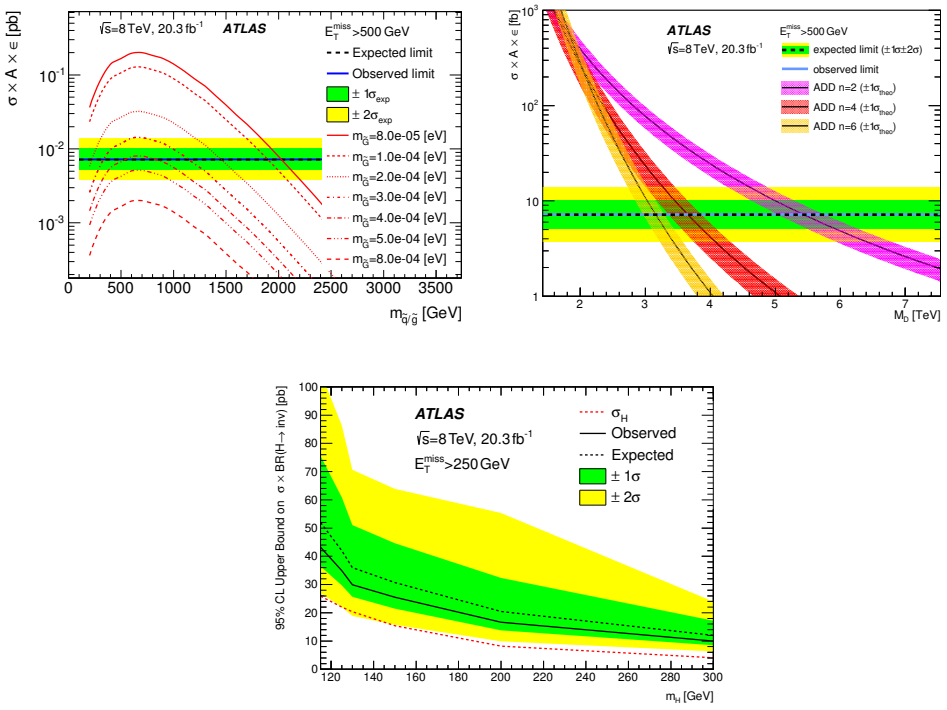

FIGURE 5. Top: comparison between the model independent results and the supersymmetric degenerate squarks and gluinos scenarios in which $pp \to \tilde{G}\tilde{g}(\tilde{q}) + X \to \tilde{G}\tilde{G}g(q)$ (top-left) and LED interpretation varying the number of dimensions n (top-right). Bottom: cross section times branching ratio limit in the Higgs invisible decay scenario as a function of the Higgs mass m_H. The expectation for a Higgs boson with BR($H \to$ inv) = 1 is also plotted. More informations in the text. Taken from Ref. [3].

universe and a considerable fraction of the branching ratio to invisible particles could be interpreted in terms of the DM production. In Figure 5 the results are translated into 95% CL limits on the production cross section times the branching ratio for a Higgs boson decaying into invisible particles as a function of the boson mass. The expectation for a Higgs boson decaying completely in the invisible sector is also plotted.

First analysis of $\sqrt{s} = 13$ TeV data

The Run-2 analysis follows a similar strategy of the one already performed with the Run-1 statistics adapting the criteria selection on the data at the new center of mass energy and bunch crossing frequency. For these reason a new object selection is applied and a new definition of the Signal and Control regions are performed.

In Figure 6 are shown the firsts results based on 68-78 pb^{-1} of collision data at $\sqrt{s} = 13$ TeV [10]. The left plot shows the muon CR defined using "relaxed" $E_{\mathrm{T}}^{\mathrm{miss}}$ and jet p_{T} cuts with respect to the Run-2 selection and this tests the analysis control on the background estimation. The picture on the right is a single-jet sample SR-like distribution where the jet cleaning requirements are removed to point out the importance of the good quality jet requirements. In fact the mono-jet final states would be dominated by the non-collision background (NCB) and an azimuthal structure characteristic of fake jets due to beam-induced backgrounds is visible. In order to suppress the NCB below the 1% level, an efficient jet cleaning is required with a suppression power of at least three orders of magnitude [11].

Preliminary expected results are just done at an energy collision of $\sqrt{s} = 14$ TeV showing promising prospectives for the Run-2 results. In particular the Run-2 projections in the WIMP search sector [12] in the EFT context show that it is possible to gain in sensitivity already with a few fb^{-1} of data collected, compared to the 8 TeV results. In the case where no excesses are observed, it is possible just using the Run-1 mono-jet analysis to improve the limits on the suppression scale M_* of a factor two (Figure 7).

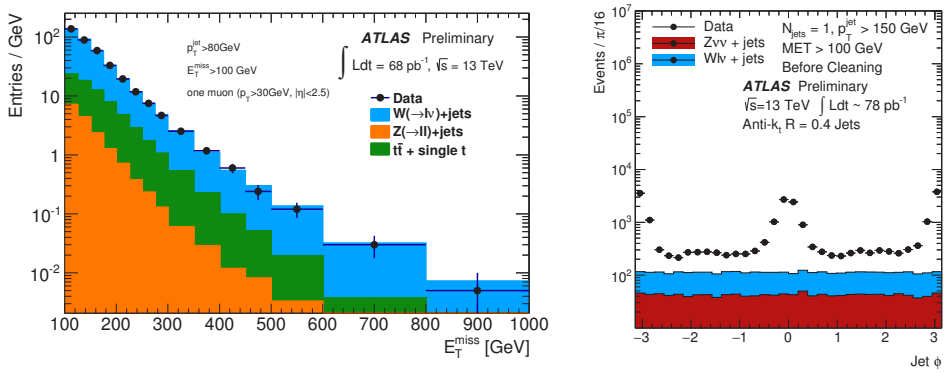

FIGURE 6. On the left: $E_{\mathrm{T}}^{\mathrm{miss}}$ distribution in the one muon Control Region of the mono-jet analysis with $E_{\mathrm{T}}^{\mathrm{miss}} > 100$ GeV and jet $p_{\mathrm{T}} > 80$ GeV cuts, showing 68 pb^{-1} of data at $\sqrt{s} = 13$ TeV. The MC predictions for SM backgrounds are normalised to data. On the right: The jet phi distribution for a single-jet sample selected with $E_{\mathrm{T}}^{\mathrm{miss}} > 100$ GeV and jet $p_{\mathrm{T}} > 150$ GeV The MC prediction corresponds to $Z(\nu\nu)$ + jets and $W(\ell\nu)$ + jets processes, normalised to the luminosity of the sample, which is measured to be 78 pb^{-1}. Additional collision processes, contributing at the 10% level or lower, are neglected. Taken from Ref. [10].

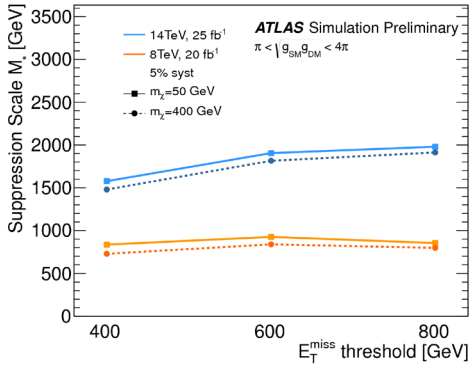

FIGURE 7. The 95% CL lower limits on the suppression scale M_* from 20 fb^{-1} at $\sqrt{s} = 8$ TeV, and 25 fb^{-1} at $\sqrt{s} = 14$ TeV. The limits for the vector operators with $m_\chi = 50$ and 400 GeV are shown for three signal regions defined by $E_{\mathrm{T}}^{\mathrm{miss}} > 400$, 600 and 800 GeV, considering 5% systematic uncertainty on Standard Model background. The 8 TeV limits presented are based on simulation only. These results assume that the EFT is a valid approach. Taken from Ref. [12].

Conclusions

The mono-jet topology constitutes a clean and distinctive signature in search of new phenomena that escape from the direct detection at colliders. Promising prospects at the new energy are estimated in all the theoretical scenarios in this analysis. As shown in the firsts Run-2 mono-jet results, the analysis is ready to use the new data thanks also to the excellent detector performance and it is ready to intepret its results in all the theoretical scenarios previoulsy cited in particular increasing the commitment in the dark sector probing a wide spectrum of possible signal hypotheses in the simplified model approach [9].

To conclude, the last results at $\sqrt{s} = 8$ TeV are in agreement with the SM predictions but with the start of Run-2 at LHC, working at the never reached centre of mass energy proton-proton collision of 13 TeV, a wide spectrum of New Physics beyond the Standard Model scenarios could be opened and the mono-jet analysis is ready to give its crucial contribution with the hope of finding a solution to the questions still open in the cosmological and particle physics fields.

REFERENCES

[1] G. Bertone, D. Hooper, and J. Silk, Phys.Rept.405:279-390,2005.
[2] G. Steigman and M. S. Turner, Nucl. Phys. **B253** (1985) 375.
[3] ATLAS Collaboration, Eur. Phys. J. C **75** (2015) 7, 299
[4] ATLAS Collaboration, JINST **3**, S08003 (2008).
[5] ATLAS Collaboration, Eur. Phys. J. **C 72** (2012) 1849.
[6] M. Klasen and G. Pignol, Phys. Rev. **D 75** (2007) 115003.
[7] N. Arkani-Hamed, S. Dimopoulos, and G. Dvali, Phys. Lett. **B 429** (1998) 263.
[8] ATLAS Collaboration, Phys. Rev. Lett. **112** (2014) 201802.
[9] D. Abercrombie *et al.*, arXiv:1507.00966 [hep-ex].
[10] ATLAS Collaboration, EXOT-2015-005, https://atlas.web.cern.ch/Atlas/GROUPS/PHYSICS/PLOTS/EXOT-2015-005/.
[11] ATLAS Collaboration, ATLAS-CONF-2015-029, https://cds.cern.ch/record/2037702
[12] ATLAS Collaboration, ATL-PHYS-PUB-2014-007, https://atlas.web.cern.ch/Atlas/GROUPS/PHYSICS/PUBNOTES/ATL-PHYS-PUB-2014-007/.